THE JOURNAL OF BIOLOGICAL CHEMISTRY VOL. 291, NO. 38, pp. 19953–19961, September 16, 2016

Epsin N-terminal Homology Domain (ENTH) Activity as a Function of Membrane Tension*

Received for publication, April 8, 2016, and in revised form, July 21, 2016 Published, JBC Papers in Press, July 27, 2016, DOI 10.1074/jbc.M116.731612

Martin Gleisner[‡], Benjamin Kroppen[§], Christian Fricke[‡], Nelli Teske[‡], Torben-Tobias Kliesch[¶], Andreas Janshoff[¶‖], Michael Meinecke[§1], and Claudia Steinem[‡‖2]**

*From the [‡]Institute of Organic and Biomolecular Chemistry, University of Göttingen, Tammannstrasse 2, 37077 Göttingen, Germany, [§]Department of Cellular Biochemistry, University of Göttingen, Humboldtallee 23, 37073 Göttingen, Germany, **European Neuroscience Institute, 37073 Göttingen, Germany, [¶]Institute of Physical Chemistry, University of Göttingen, Tammannstrasse 6, 37077 Göttingen, Germany, and [‖]Göttingen Center for Molecular Biosciences, 37077 Göttingen, Germany*

The epsin N-terminal homology domain (ENTH) is a major player in clathrin-mediated endocytosis. To investigate the influence of initial membrane tension on ENTH binding and activity, we established a bilayer system based on adhered giant unilamellar vesicles (GUVs) to be able to control and adjust the membrane tension σ covering a broad regime. The shape of each individual adhered GUV as well as its adhesion area was monitored by spinning disc confocal laser microscopy. Control of σ in a range of 0.08-1.02 mN/m was achieved by altering the Mg^{2+} concentration in solution, which changes the surface adhesion energy per unit area of the GUVs. Specific binding of ENTH to phosphatidylinositol 4,5-bisphosphate leads to a substantial increase in adhesion area of the sessile GUV. At low tension (<0.1 mN/m) binding of ENTH can induce tubular structures, whereas at higher membrane tension the ENTH interaction deflates the sessile GUV and thereby increases the adhesion area. The increase in adhesion area is mainly attributed to a decrease in the area compressibility modulus K_A. We propose that the insertion of the ENTH helix-0 into the membrane is largely responsible for the observed decrease in K_A, which is supported by the observation that the mutant ENTH L6E shows a reduced increase in adhesion area. These results demonstrate that even in the absence of tubule formation, the area compressibility modulus and, as such, the bending rigidity of the membrane is considerably reduced upon ENTH binding. This renders membrane bending and tubule formation energetically less costly.

Clathrin-mediated endocytosis is one of the key metabolic pathways for the uptake of macromolecules into eukaryotic cells (1–4). Driven by a chain of remodeling events and an elaborate set of proteins acting in an orchestrated manner, an almost flat patch of plasma membrane is transformed into a closed, cargo-containing vesicle. As plasma membrane shape transformation is associated with significant local bending of the membrane, the process is highly sensitive to lateral membrane tension. Plasma membrane tension originates from two primary sources; that is, hydrostatic pressure across the lipid bilayer and cytoskeleton-membrane adhesion (5). Depending on the cell type, plasma membrane tensions span a range of roughly 0.003–0.45 mN/m (5–8). Even though it had become clear already in the late 1990s that tension plays a role in exo- and endocytosis (9, 10), only in recent years has significant evidence been accumulated that membrane tension is of utmost importance for processes that rely on membrane remodeling (11–14). Cells actively maintain and regulate their membrane tension and use it to control exo- and endocytosis (15). In K562 cells it has been reported that endocytosis is completely suppressed under hypoosmotic conditions (16). Generally, high lateral membrane tension suppresses membrane deformation as both stretching the lipid bilayer and opening bonds between the cytoskeleton and the plasma membrane requires a large amount of energy (17).

One protein domain that is involved in endocytosis is the epsin N-terminal homology domain (ENTH) (18, 19). It is known that ENTH of epsin-1 binds specifically to the receptor lipid PtdIns(4,5)P_2 (20–22), resulting in tubulation or even vesiculation (23, 24) as a result of membrane bending. Upon binding to PtdIns(4,5)P_2 an additional α-helix, referred to as helix-0 (amino acids 3–15) at the N terminus of ENTH, is formed. This newly formed helix-0 inserts into the inner monolayer of the plasma membrane resulting in an asymmetry that produces membrane curvature (25, 26). By means of protruded pore-spanning membranes exhibiting a lateral tension of ~2 mN/m, we recently showed that specific ENTH binding to PtdIns(4,5)P_2-containing membranes reduces membrane tension (27). However, ENTH-induced tubulation was never observed. We thus asked the question, whether the initial lateral membrane tension influences the process that is initiated by ENTH- PtdIns(4,5)P_2 interaction.

To control lateral membrane tension in an artificial well defined membrane system, we made use of giant unilamellar vesicles (GUVs) that adhere to an avidin-coated glass substrate. By adjusting the Mg^{2+} concentration in solution, we were able to control and tune the lateral membrane tension of these GUVs in a range of 0.08–1.02 mN/m. These values are well below the tension value of 2 mN/m reported in the

* This work was supported by DFG (Deutsche Forschungsgemeinschaft; SFB 803, projects B04, B08, and B09). The authors declare that they have no conflicts of interest with the contents of this article.
[1] To whom correspondence may be addressed: Dept. of Cellular Biochemistry, University of Göttingen, Humboldtallee 23, 37073 Göttingen, Germany. Tel.: 49551-398189; Fax: 49551-3395979; E-mail: michael.meinecke@med.uni-goettingen.de.
[2] To whom correspondence may be addressed: Institute of Organic and Biomolecular Chemistry, University of Göttingen, Tammannstr. 2, 37077 Göttingen, Germany. Tel.: 49551-3933294; Fax: 49551-3933228; E-mail: csteine@gwdg.de.

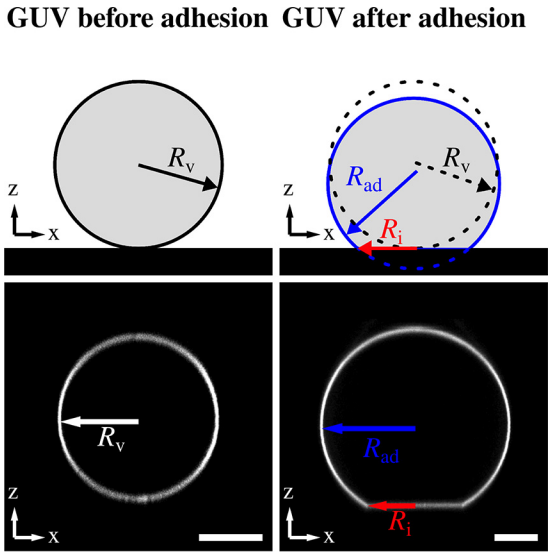

FIGURE 1. **Scheme of an adhered GUV.** Shown is a schematic drawing (*top images*) and corresponding SDCLM images (*bottom images*) of a GUV on an avidin-coated surface before and after adhesion. Without adhesion, the GUV geometry can be approximated as a sphere (radius R_v). After adhesion, a spherical cap with a radius of R_{ad} and a circular contact area (with a radius of R_i) is formed. *Scale bars*: 10 μm.

previous study (27) and might allow monitoring ENTH-induced membrane changes including tubulation or vesiculation. We show that with this system in hand, binding and helix-0 insertion of ENTH can be monitored in a label-free fashion by determining the increase in adhesion area of the GUV. From our observations, we conclude that ENTH binding results in a substantial softening of the lipid bilayer, which can eventually result in tubule formation at low initial lateral tension.

Results and Discussion

Tuning the Adhesion of GUVs by Mg^{2+}—Fluorescently labeled GUVs composed of DOPC/DOPE/Atto488 DPPE[3] were doped with *N*-(cap-biotinyl)-DOPE to attach them onto the avidin-coated glass surface (28). For specific binding of ENTH to GUVs, the natural receptor lipid PtdIns(4,5)P_2 with a concentration of 0.8 mol% was supplemented. To obtain the shape of the vesicles, they were imaged by spinning disc confocal laser microscopy (SDCLM) (Fig. 1, *bottom images*). Attractive forces between the GUV and the avidin-coated surface change its shape from a sphere with a radius R_v to a spherical cap with a slightly increased radius of the cap denoted as R_{ad} (Fig. 1, *top images*). The spherical cap geometry is indicative of the strong adhesion regime (29, 30). In the limit of strong adhesion the bending energy associated with changes in the shape of the vesicle can be ignored, and the vesicle can be described as a spherical cap usually parameterized solely by the contact angle Θ with the surface (30, 31). The adhered GUV forms a circular contact area with the functionalized glass substrate with a radius R_i (Fig. 1, *top image*) (32). This adhesion area increases until the free energy of the vesicle is minimized. The elastic energy encompasses stretching energy, bending energy, and the entropic cost of suppressing thermal fluctuations of the contact area between the GUV and the substrate (33). Adhesion energy is obtained from the surface energy times the contact area. In the strong adhesion limit, we can safely assume that the free energy F_v comprises only an elastic stretching term and an adhesion term (Equation 1),

$$F_v = \frac{1}{2} K_A \frac{(A_{ad} - A_v)^2}{A_v} - A_i \gamma_{ad} \qquad \text{(Eq. 1)}$$

where K_A is the area compressibility modulus of the bilayer, A_{ad} is the area of the adhered vesicle, A_v is the area of the free vesicle, A_i is the contact area, and γ_{ad} is the adhesion energy per unit area mainly originating from bond formation between a GUV and the substrate. Minimization of the free energy assuming constant volume requires the shell to be laterally dilated to allow generation of a finite-sized adhesion zone (31). Naturally, stretching of the bilayer inevitably generates lateral tension. Therefore, controlling the adhesion area permits to adjust membrane tension.

To modify the contact area of a GUV, we made use of the fact that divalent cations increase the membrane-surface interaction, *i.e.* it was found that a strong interaction between phosphatidylcholine and Mg^{2+} promotes spreading of vesicles to planar supported bilayers (34–36). To adjust the Mg^{2+} concentration, GUVs formed in sucrose solution (298 mosmol/kg) were added to a sucrose-containing buffer solution (2 mM HEPES, sucrose, pH 7.4, 298 mosmol/kg) doped with different $MgCl_2$ concentrations. Isoosmolar conditions are required as the size of the contact area is also a function of the GUV excess area, which depends on the osmolality gradient. GUVs were allowed to bind to the avidin-coated surface and were imaged by SDCLM. Fig. 2 illustrates the increase in contact area of GUVs doped with 0.8 mol% PtdIns(4,5)P_2 as a function of Mg^{2+} concentration. To compare GUVs of different sizes, the radius R_i of the contact area was related to the radius R_{ad} of the adhered GUV (Fig. 2). This allowed us to normalize the adhesion area to the size of the GUV and compare different ensembles. The increase of R_i/R_{ad} with Mg^{2+} concentration (Fig. 3) suggests that Mg^{2+} promotes the adhesion of the GUVs by interaction of the lipid head groups of the membrane with the functionalized glass surface (34, 37). In addition to this interaction, it is also conceivable that Mg^{2+} influences the biotin-avidin-interaction itself. Holmberg *et al.* (38) showed that the dissociation of a biotin-streptavidin bond strongly depends on the ionic strength and is almost fully prevented in the presence of Mg^{2+}. In essence, both effects result in a larger contact area with increasing Mg^{2+} concentration.

Estimating Lateral Membrane Tension from the Contact Area—The observed contact area of the GUV with the glass surface provides information about the lateral tension of the GUV membrane. Assuming constant volume of the GUV during the course of the experiment due to the low water permeability of the membrane (39) and isoosmolar conditions, lateral

[3] The abbreviations used are: Atto488 DPPE, Atto488-1,2-dipalmitoyl-*sn*-glycero-3-phosphoethanolamine; DOPC, 1,2-dioleoyl-*sn*-glycero-3-phosphocholine; DOPE, 1,2-dioleoyl-*sn*-glycero-3-phosphoethanolamine; ENTH, epsin N-terminal homology domain; GUV, giant unilamellar vesicle; cap-biotin-PE, 1,2-dioleoyl-*sn*-glycero-3-phosphoethanolamine-*N*-(cap biotinyl); PtdIns(4,5)P_2, 1,2-dioctanoyl-*sn*-glycero-3-phospho-(1′-myo-inositol-4′,5′-bisphosphate); SDCLM, spinning disc confocal laser microscopy.

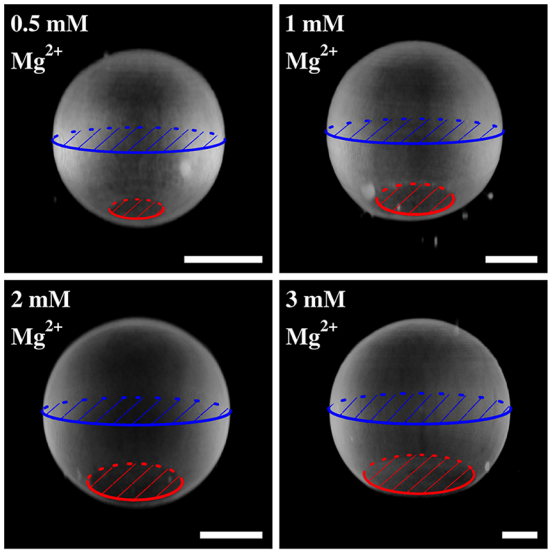

FIGURE 2. **Vesicle contact area as a function of Mg^{2+} concentration.** Representative three-dimensional reconstructions of SDCLM images of GUVs (DOPC/DOPE/cap-biotin-PE/Atto488-DPPE/PtdIns(4,5)P_2, 66.2:30:2:1:0.8) adhering on an avidin-coated glass surface. Adhesion strength is modulated by different Mg^{2+} concentrations. The ratio of the contact area (*red*) to the equatorial plane (*blue*) of a GUV is a function of the Mg^{2+} concentration. *Scale bars*: 10 μm.

tension can be computed from the area dilatation generated by adhesion. In equilibrium, larger adhesion forces generate larger area dilatation. To calculate the lateral membrane tension from the normalized area increase, one has to consider two contributions, one from ironing out membrane undulations and one from dilating a flat membrane laterally in a two-dimensional Hookean fashion (40). Excess area stored in thermally excited membrane undulations is sacrificed first followed by lateral expansion of lipids. Equation 2 relates area dilatation to membrane tension σ of an adhered GUV (41),

$$\frac{\Delta A}{A_v} = \frac{\sigma - \sigma_0}{K_A} + \frac{k_B T}{8\pi\kappa} ln\left(\frac{\sigma}{\sigma_0}\right) \quad \text{(Eq. 2)}$$

The bending rigidity κ of a DOPC membrane is assumed to be 21 $k_B T$, and the area compressibility modulus $K_A = 265$ mN/m accordingly (42). As a reference state, we choose the free vesicle with tension σ_0, which depends on the size of the vesicle and the osmotic pressure between inside and outside of the vesicle. Equation 2 holds, if $\sigma_0 \ll \sigma$, and allows the estimation of the lateral membrane tension σ of an adhered GUV numerically. Because it is impossible to determine σ_0 for all vesicles used here independently, we determined σ_0 for a few representative GUVs by parallel plate compression in conjunction with optical microscopy (43). We found σ_0 to be in the range of 10^{-6}-10^{-4} N/m in accordance with typical values for weakly adhering GUVs on a glass substrate as obtained by reflectometric interference microscopy (44).

To calculate the tension σ, we need to determine the relative area dilatation after adhesion of the vesicle. A free GUV forms a sphere with an area A_v. It changes its geometry upon adhesion and forms a spherical cap with an increased surface area A_{ad}. Note that a spherical cap geometry corresponds to the limit of strong adhesion with respect to membrane undulations (29).

The normalized change in surface area $\Delta A/A_v$ can be calculated from the shape change (Equation 3),

$$\frac{\Delta A}{A_v} = \frac{A_{ad} - A_v}{A_v} = \frac{4\pi R_{ad}^2 + \pi R_i^2 - 2\pi R_{ad}(R_{ad} - \sqrt{R_{ad}^2 - R_i^2}) - 4\pi R_v^2}{4\pi R_v^2} \quad \text{(Eq. 3)}$$

with the condition of constant volume,

$$\frac{4\pi}{3} R_v^3 = \frac{4\pi}{3} R_{ad}^3 - \frac{\pi(R_{ad} - \sqrt{R_{ad}^2 - R_i^2})}{6}(3R_i^2 + (R_{ad} - \sqrt{R_{ad}^2 - R_i^2})^2) \quad \text{(Eq. 4)}$$

$\Delta A/A_v$ is only a function of R_i/R_{ad}, which is related to the contact angle between a sessile vesicle and the substrate by $\Theta = \sin^{-1}(R_i/R_{ad})$.

Fig. 3 shows the R_i/R_{ad} values ($n_{total} = 467$) of adhered PtdIns(4,5)P_2 containing GUVs with an average radius of $R_v = 18 \pm 5$ μm for different Mg^{2+} concentrations. The mean ratios of R_i/R_{ad} increased from 0.46 at a Mg^{2+} concentration of 0.5 mM to 0.63 at 3.0 mM. For GUVs lacking PtdIns(4,5)P_2 ($n_{total} = 413$) with an average radius of $R_v = 18 \pm 5$ μm, R_i/R_{ad} increased from 0.19 at a Mg^{2+} concentration of 1 mM to 0.53 at 6.0 mM. Fig. 4 shows how area dilatation and lateral tension change as a function of R_i/R_{ad} according to Equations 2, 3 and 4.

Based on this theoretical framework, the lateral tension of GUVs composed of DOPC/DOPE/cap-biotin-PE/Atto488-DPPE/PtdIns(4,5)P_2 (66.2:30:2:1:0.8) adhering to an avidin-coated glass surface using different Mg^{2+} concentrations can be calculated (Fig. 5). The mean tensions cover a range of 0.08–1.02 mN/m assuming $\sigma_0 = 10^{-5}$ N/m. The upper value is slightly larger than values found for cell membranes, which range between 0.003 and 0.45 mN/m (5–8).

A small change in R_i/R_{ad} can result in a rather large change in lateral membrane tension (Fig. 4). At low R_i/R_{ad}, the excess area of the GUV stored in undulations compensates for the area dilation caused by adhesion on the surface ($R_i/R_{ad} = 0.46$, $\sigma = 0.08$ mN/m), whereas for larger R_i/R_{ad} undulations are ironed out, and the lateral membrane tension increases significantly due to the first term in Equation 2 ($R_i/R_{ad} = 0.63$, $\sigma = 1.02$ mN/m). The results clearly demonstrate that the lateral membrane tension of adhered GUVs can be readily adjusted within a certain regime making use of different Mg^{2+} concentrations to control γ_{ad}, the adhesion energy per unit area. This system thus enables us to study the influence of the specific binding of ENTH to PtdIns(4,5)P_2 containing GUVs as a function of a given initial lateral membrane tension.

ENTH Binding to PtdIns(4,5)P_2-doped GUVs—ENTH can induce membrane tubulation (22, 25). Recently we showed that binding of ENTH to PtdIns(4,5)P_2-doped and slightly curved pore-spanning membranes results in a reduction of the lateral membrane tension (27). However, the initial tension of the bilayer was rather high, and it is well conceivable that tubulation is suppressed at elevated tension. To answer the question of how ENTH binding to PtdIns(4,5)P_2 containing adhered

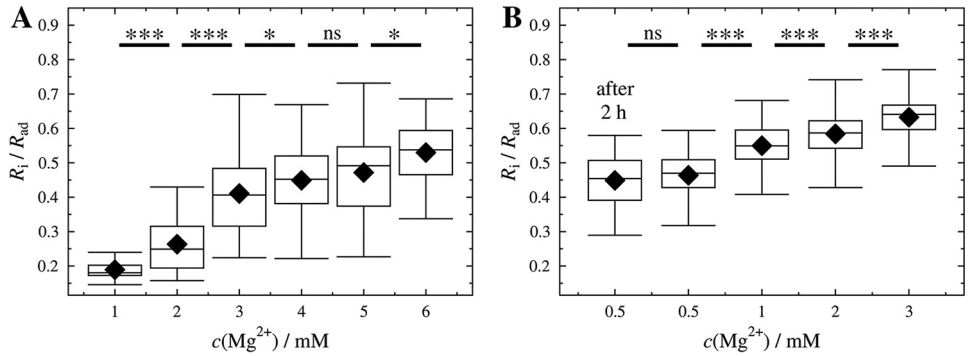

FIGURE 3. **Ratios R_i/R_{ad} as a function of Mg^{2+} concentration.** Ratios of contact radius to initial vesicle radius R_i/R_{ad} of GUVs composed of DOPC/DOPE/cap-biotin-PE/Atto488-DPPE (67:30:2:1) (*A*) and DOPC/DOPE/cap-biotin-PE/Atto488-DPPE/PtdIns(4,5)P_2 (66.2:30:2:1:0.8) (*B*) adhered to an avidin-coated glass surface measured at different Mg^{2+} concentrations. For each condition 31–101 GUVs (n_{total} = 413, *A*) and 79–117 GUVs (n_{total} = 467, *B*) were measured obtained from at least two independent preparations for each condition. After 2 h of incubation the same values were obtained (see in *B*, after 2 h). *Black diamonds* represent the mean. ***, $p < 0.001$; *, $p < 0.05$; *ns*, not significant.

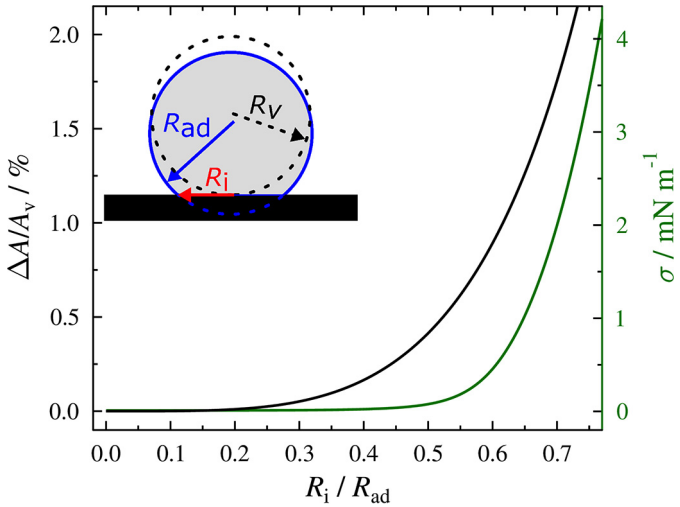

FIGURE 4. **Normalized area dilatation $\Delta A/A_v$ as a function of R_i/R_{ad}.** The theoretically calculated relationship of the normalized area dilatation ($\Delta A/A_v$) as a function of R_i/R_{ad} according to Equations 1 and 2 is shown as a *solid black line*. The lateral tension resulting from the area dilatation was calculated using Equation 3 and 4 with K_A = 265 mN/m, κ = 21 k_BT and $\sigma_0 = 10^{-5}$ N/m (*green line*).

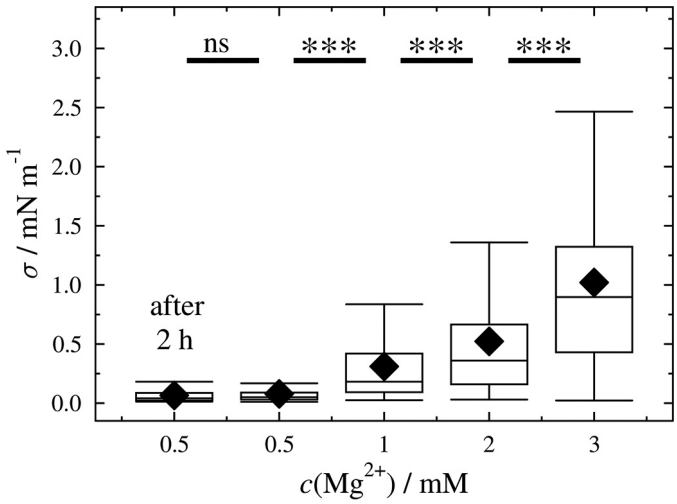

FIGURE 5. **Calculated membrane tension as a function of Mg^{2+} concentration.** Lateral membrane tension of GUVs (DOPC/DOPE/cap-biotin-PE/Atto488-DPPE/PtdIns(4,5)P_2, 66.2:30:2:1:0.8) adhering on an avidin-coated glass surface obtained at different Mg^{2+} concentrations. The mean tensions at different Mg^{2+} concentrations are: 0.08 mN/m (0.5 mM), 0.31 mN/m (1 mM), 0.52 mN/m (2 mM), and 1.02 mN/m (3 mM). For each condition 79–117 GUVs were measured (n_{total} = 467). After 2 h of incubation the same values were obtained (after 2 h). *Black diamonds* represent the mean. ***, $p < 0.001$; ns, not significant.

GUVs alters their shape dependent on the preadjusted lateral membrane tension, we prepared GUVs composed of DOPC/DOPE/cap-biotin-PE/Atto488-DPPE/PtdIns(4,5)P_2, (66.2:30:2:1:0.8) in the presence of 0.5 mM and 2 mM Mg^{2+}. The resulting mean membrane tensions were 0.08 mN/m and 0.52 mN/m, respectively. To these adhered GUVs, ENTH was added at a final concentration of c_{ENTH} = 1 μM. Interestingly, dependent on the preadjusted lateral membrane tension, two different behaviors were observed after protein addition. At a low lateral membrane tension (σ = 0.08 mN/m), the addition of ENTH can indeed result in the formation of tubules, eventually leading to the disappearance of the GUV (Fig. 6). Because of the stirring of the solution, tubules appear preferentially on one side of the GUV and also elongated along this direction. Of note, even at this low lateral membrane tension, only part of the GUVs show tubulation, whereas others display an increase in adhesion area indicative of transient reduction in lateral membrane tension (see below).

It has been shown that upon binding of ENTH to PtdIns(4,5)P_2, the protein experiences a change in structure in which helix-0 inserts into the lipid bilayer as demonstrated by EPR spectroscopy (22). This increases the surface area of the outer leaflet of the GUV membrane and induces an asymmetry in the two bilayer leaflets facilitating membrane bending by generating spontaneous curvature (26, 45). In agreement with our observations of tubule formation upon ENTH binding, association of full-length epsin and ENTH to non-adhered tension-free GUVs also resulted in the formation of irregular structures such as vesicles and tubules (23, 25, 46, 47) dependent on the experimental conditions and on the surface density of bound protein (48, 49). Recently, Shi and Baumgart (49) provided experimental evidence for a mechanism whereby local membrane tension reduction mediated by endocytic proteins reduces the elastic energy required for membrane deformation and thus facilitates membrane budding and tubulation. Molecular dynamics simulations predicted that the formation of tubules requires a lower protein coverage on the membrane than the formation of vesicles (48). To calculate the protein surface coverage in this

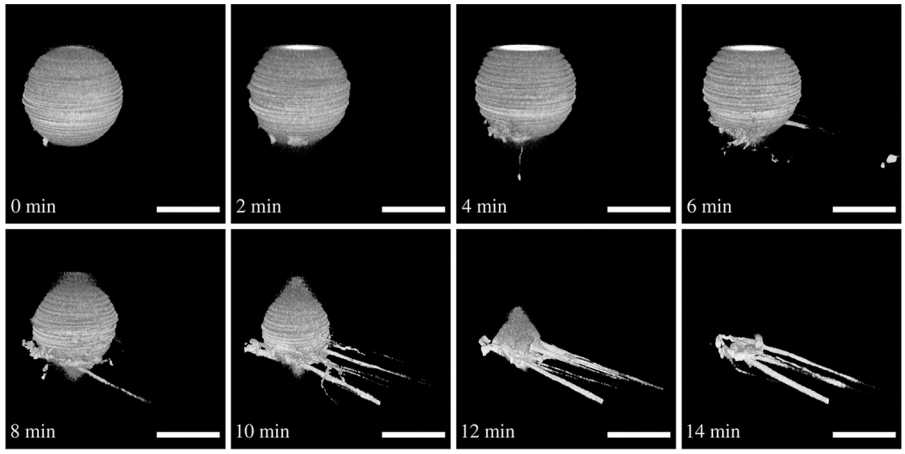

FIGURE 6. **Tubulation after ENTH binding to a GUV with low membrane tension.** Time series of three-dimensional reconstructions of SDCLM images of a GUV (DOPC/DOPE/cap-biotin-PE/Atto488-DPPE/PtdIns(4,5)P_2, 66.2:30:2:1:0.8) adhering on an avidin-coated glass surface at low membrane tension ($c(Mg^{2+}) = 0.5$ mM). The GUV starts to tubulate after ENTH addition ($c_{ENTH} = 1$ μM) and forms tethers until all lipid material is dissipated. Tubulation starts at $t =$ 0 min. *Scale bars*: 10 μm.

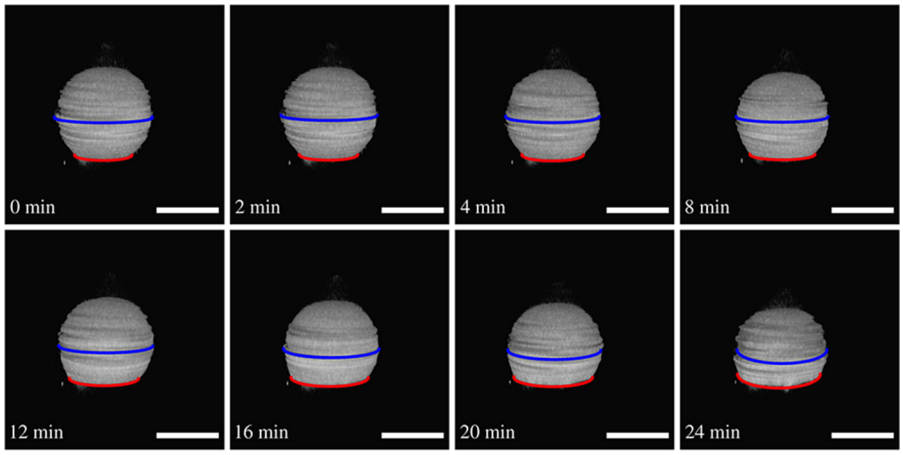

FIGURE 7. **Flattening of a GUV with elevated membrane tension after ENTH binding.** Time series of three-dimensional reconstructions of SDCLM images of a GUV (DOPC/DOPE/cap-biotin-PE/Atto488-DPPE/PtdIns(4,5)P_2, 66.2:30:2:1:0.8) adhering on an avidin-coated glass surface generating high membrane tension ($c(Mg^{2+}) = 2$ mM). The GUV starts to flatten after ENTH addition ($c_{ENTH} = 1$ μM), and R_i/R_{ad} increases. Flattening starts at $t = 0$ min. *Scale bars*: 20 μm.

study, we determined the dissociation constant of ENTH to PtdIns(4,5)P_2-doped planar POPC membranes (9:1) by reflectometric interference spectroscopy, which resulted in a $K_D =$ 0.8 μM. This in turn means that at an ENTH concentration of 1 μM, 56% of the receptor lipids are occupied. The GUVs used in this study contain 0.8% of the receptor lipid PtdIns(4,5)P_2. Taking the protein's footprint of 16 nm^2 (50) into account and assuming a 1:1 binding of ENTH to PtdIns(4,5)P_2 results in a protein surface coverage on the membrane of 10%. This rather low protein coverage agrees with the observation that only tubules are formed and no vesicles (50, 51).

However, if GUVs with a larger membrane tension of $\sigma =$ 0.52 mN/m was incubated with ENTH, in none of the cases was tubulation observed. Instead, the adhered vesicles started to flatten, and their contact area increased after ENTH binding (Fig. 7), *i.e.* the distance between the equatorial plane of the GUV (Fig. 7, *blue line*) and its contact area (Fig. 7, *red line*) was reduced as a function of time. The size of the adhesion area is a result of the newly established equilibrium between adhesion force and membrane tension (33). When the new equilibrium was adjusted after ENTH binding, the membrane tension again reached its previous value of $\sigma = 0.52$ mN/m, which essentially prevents tubule formation as any deformation would require further dilation of the membrane as long as the volume is conserved.

This unique experimental approach allowed us to obtain statistically meaningful data by imaging 10s of GUVs before and after protein addition as a function of membrane tension. Normalized contact radii R_i/R_{ad} of GUVs adhered to an avidin-coated substrate at three different Mg^{2+} concentrations were imaged by SDCLM before and after incubation with ENTH for 1 h to ensure equilibrium conditions. Fig. 8 clearly shows that for each Mg^{2+} concentration the ratio of R_i/R_{ad} is significantly larger after ENTH addition (Fig. 8, *gray boxes*) than before (Fig. 8, *white boxes*). For low membrane tension, where also tubulation can occur, only those GUVs with no indication of tubulation were used for statistical analysis.

Under the assumptions that the adhesion energy per unit area remains the same and the initial tension is restored after insertion of the proteins' helix-0, an increase in R_i/R_{ad} can only be explained by an area increase δA_{ENTH} upon helix-0 insertion or by a decrease of the area compressibility modulus $K_{A,ENTH}$

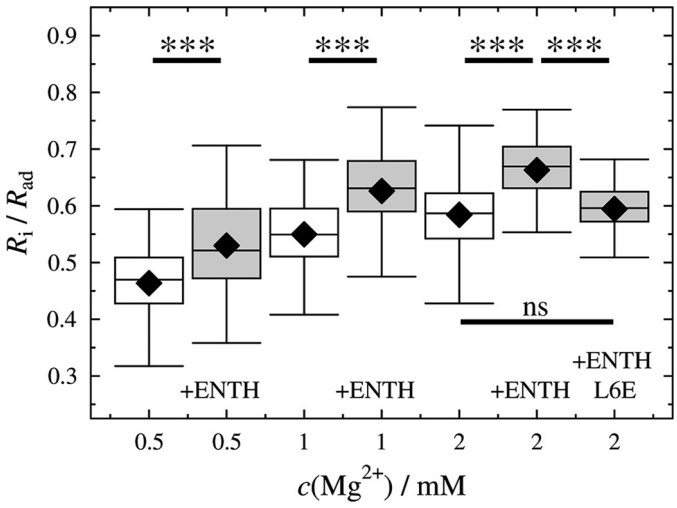

FIGURE 8. **Changes in R_i/R_{ad} in response to ENTH binding as a function of initial membrane tensions.** R_i/R_{ad} of GUVs adhering on an avidin-coated glass surface measured at different Mg^{2+} concentrations before and after ENTH addition (c_{ENTH} = 1 μM). For each condition 52–117 GUVs were measured obtained from at least two independent preparations; *black diamonds* represent the mean; n_{total} = 556. ***, $p < 0.001$; *ns*, not significant.

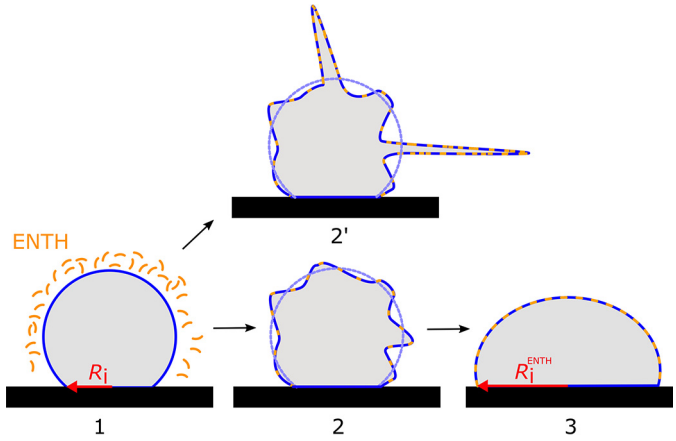

FIGURE 9. **Model of ENTH action.** Insertion of helix-0 into a sessile vesicle (*1*) relaxes its tension until either tubulation sets in at low initial tension (2′) or a new equilibrium state is established (*3*) that requires to produce a larger adhesion area.

(for details see "Appendix"). First, we estimate the expected increase in area δA_{ENTH} due to helix insertion. Therefore, we take the area of helix-0 of ENTH into account, which is ~10–30% (= 1.6–4.8 nm^2) of the ENTH surface projection. Employing the determined dissociation constant K_D and the known PtdIns(4,5)P_2 concentration assuming a PtdIns(4,5)P_2 area of 0.7 nm^2 (52) in the GUVs, this translates into a maximal expected relative area increase of 1–3%. Next, we compare this estimate with the experimentally obtained relative area change deduced from the measured changes in R_i/R_{ad} before and after ENTH binding. Under the assumption that the adhesion energy per unit area of the GUV and its volume remain constant, a relative area increase of 83% is calculated (see "Appendix"). The computed relative area increase is independent of the initial tension. Such a tremendous area increase is unrealistic and contradicts the theoretically expected relative area increase. Thus, we conclude that δA_{ENTH} does not explain the significant change in R_i/R_{ad}. Instead, a substantially reduced area compressibility modulus K_A might explain the observation. Neglecting in this case the area increase of δA_{ENTH} due to insertion alone and calculating the altered K_A values, one finds that K_A reduces from the initial value of K_A = 265 mN/m to 145 mN/m independent of the initial lateral membrane tension.

We speculate that the insertion of helix-0 of ENTH into one leaflet of the membrane is responsible for the observed reduction in K_A. To confirm this hypothesis, we performed the same GUV experiments at 2 mM Mg^{2+} but replaced wild type ENTH with the mutant ENTH L6E. This mutant binds Ins(1,4,5)P_3 with the same affinity constant as the wild type but has a reduced binding affinity to short chain diC8PtdIns(4,5)P_2 and does not induce tubules in vesicles (23, 25). The result depicted in Fig. 8 demonstrates that the change in R_i/R_{ad} is significantly smaller than that observed for wild type ENTH, suggesting that helix-0 is largely responsible for the observed change in K_A. A reduction in K_A directly translates into a reduction of the bending rigidity κ, *i.e.* ENTH binding accompanied by helix-0 insertion reduces the energetic cost for bending and thus tubule formation.

Membrane softening has been shown to occur upon interaction of several small peptides with membranes and has been ascribed to perturbations on the membrane organization and to a direct modulation of κ by membrane thinning (53–55). Settles *et al.* (53) showed that Sar1p, a protein involved in vesicle trafficking, dramatically lowers the rigidity of lipid bilayer membranes. This membrane softening does not rely on the imposition of strong local curvature and is a profoundly different mode of action than those typically ascribed to intracellular curvature-associated proteins. For ENTH, elasticity theory predicts curvature generation based on membrane insertion of helix-0 (56), which can occur on the local scale. In our setup, membrane softening due to helix-0 coupled to the local curvature of the membrane led either to tubule formation, if this process is faster than the adjustment of the new equilibrium state of the GUVs, or to an increase in R_i/R_{ad} if tubule formation is slower. In contrast, GUVs with a larger initial tension do not become floppy enough so that local curvature did not lead to tubule formation. Instead, the GUVs reached the new equilibrium state upon membrane softening, observable as an increased R_i/R_{ad}. It is conceivable that this is a kinetic effect, *i.e.* the GUV spreads faster regaining its initial tension than tubules can be formed. As the amount of bound ENTH is largely given by the mole fraction of the receptor lipid PtdIns(4,5)P_2, the reduction in K_A, κ is independent of the initial lateral membrane tension as expected. Fig. 9 proposes a model based on our findings. Insertion of helix-0 into a prestressed vesicle (*1*) relaxes tension until either tubulation sets in at low initial tension (*2′*) or a new equilibrium state is adopted (*3*) by generating a larger adhesion area to maintain tension.

Our results are in line with a recent study of Shi and Baumgart (49). They have shown by micropipette aspiration experiments on single GUVs that a larger membrane tension of 0.25 mN/m strongly inhibits N-BAR-induced shape instability, which is required for the formation of tubules (49). N-BAR domains are found in endocytic proteins and are one of the best studied examples of proteins that sense and induce membrane

curvature and whose binding involves also the insertion of parts of the protein into the membrane (57). Molecular dynamics simulations support the findings of Baumgart and coworkers (58) showing that a membrane tension in the range of 0.2 mN/m and larger increases the free energy barrier for the formation of tubules from a planar membrane and inhibits polymerization of N-BAR domains (59). Our results as well as those of others are also in line with the notion that exo- and endocytic pathways are regulated by lateral membrane tension *in vivo*. Hypoosmotic conditions resulted in a membrane tension of 4.2 mN/m and completely suppressed endocytosis in K562 cells (16). The endocytic activity in 2H3 cells decreased after increasing the membrane tension by osmotic swelling, whereas membrane tension dropped if the cells were stimulated to secrete (10).

Conclusions—We have shown that it is possible to adjust the lateral membrane tension of GUVs adhered to an avidin-coated glass surface by varying the Mg^{2+} concentration in solution. In contrast to micropipette aspiration, where the lateral tension can be precisely adjusted, the presented method has the advantage that 10s of GUVs can be imaged simultaneously allowing for high statistics to be obtained. The influence of protein binding on the morphology of the adhered GUVs as well as on the membrane's mechanical properties can be easily inspected by confocal microscopy without the need for protein labeling. Based on our results, we propose that the insertion of helix-0 of ENTH into the membrane is largely responsible for tubule formation at low lateral tension, whereas it mainly softens the membrane at higher membrane tensions. Our findings contribute to the overall discussion about how helix-0 insertion modulates membrane curvature and mechanical properties of the membranes. We suggest that the reduction of bending rigidity of membranes plays a pivotal role in all forms of endocytosis.

Experimental Procedures

Preparation of GUVs—Lipids (Avanti Polar Lipids, Alabaster, AL) were dissolved in $CHCl_3$ in the desired ratio and deposited on indium tin oxide-coated cover slips ($V = 50$ μl, $c = 0.8$ mg/ml). After solvent removal under reduced pressure for 3 h at room temperature, GUVs were formed by electroformation (AC, 3 V, 5 Hz, 2 h) in sucrose solution (298 mosmol/kg). GUVs were composed of either DOPC/DOPE/*N*-(cap biotinyl)-DOPE/Atto488 DPPE (67:30:2:1), or DOPC/DOPE/*N*-(cap biotinyl)-DOPE/PtdIns(4,5)P_2/Atto488 DPPE (66.2:30:2:1:0.8).

Preparation of Avidin-coated Glass Slides—Glass slides (Ibidi GmbH, Planegg, Germany) were treated with a mixture of $H_2O/NH_3/H_2O_2$ (5:1:1, *v*/*v*/*v*) for 20 min at 70 °C before incubation with an avidin solution ($c = 10$ μM) dissolved in phosphate-buffered saline (PBS, 137 mM NaCl, 2.7 mM KCl, 10 mM Na_2HPO_4, 1.8 mM KH_2PO_4, pH 7.4) for 30 min at room temperature, and the glass slides were thoroughly rinsed with ultrapure H_2O. After adsorption of avidin and rinsing with buffer, the avidin-coated glass surface was passivated by incubation with bovine serum albumin (10 mg/ml) for 30 min. Afterward, the glass slides were transferred into sucrose-containing buffer (2 mM HEPES, sucrose, pH 7.4, $O_{final} = 298$ mosmol/kg) with the desired Mg^{2+} concentration.

ENTH Expression—ENTH (wild type and L6E mutant) was expressed and purified as described previously (27). ENTH of rat epsin1 (residues 1–164) fused with a glutathione *S*-transferase tag was cloned into the vector pGEX-6P-1. After protein expression in BL21 cells for 3 h at 37 °C, the cells were lysed using Emulsiflex C3 and spun at 140,000 × *g* for 30 min at 4 °C in a Beckman Ti45 rotor. The supernatant was bound to glutathione beads for 30 min. Afterward, the beads were washed 6 times with 20 mM HEPES, 150 mM NaCl, 2 mM dithiothreitol, 2 mM EDTA, pH 7.4, with 2 washes at 700 mM NaCl in between. After cleavage of the glutathione *S*-transferase tag using PreScission proteases, the cleaved proteins were further purified by gel filtration (Superdex 200). The protein was transferred into sucrose-containing buffer with the corresponding Mg^{2+} concentration using Amicon® Ultra 4 ml Filters (NMGG10000, Merck, 3 × 30 min, 4000 × *g*, 4 °C; Allegra™ X-22R, Rotor SX4250, Beckman Coulter, Krefeld, Germany).

Spinning Disk Confocal Fluorescence Setup—Fluorescence images were obtained using a spinning disc confocal microscope (spinning disc unit: Yokogawa CSU-X, Rota Yokogawa GmbH & Co. KG, Wehr, Germany; stand: Olympus custom-made, Olympus Deutschland GmbH, Hamburg, Germany; piezo nanofocusing z-drive: P-721-CDQ, Physik Instrumente GmbH & Co. KG, Karlsruhe/Palmbach, Germany; camera: iXON 897Ultra, Andor Technology Ltd., Belfast, UK) equipped with a water immersion objective CFI Plan 100XW 100 ×/1.1 (Nikon GmbH, Düsseldorf, Germany) and a custom-made humidity chamber. The humidity chamber minimized water evaporation and ensured isoosmolarity for at least 2 h. Atto 488 DPPE was excited at $\lambda = 488$ nm, and the fluorescence light was selected with a 496/LP emission filter (AHF Analysentechnik AG, Tübingen, Germany). Fluorescence microscopy images were visualized by the program IMARIS (version 8.1.2, Bitplane AG, Zürich, Switzerland). A median filter (3 × 3 × 3) was used for smoothing.

GUV Data Evaluation—To automatically determine the z-position of the contact area of the GUV, a custom-written Matlab-script was used. An intensity profile was measured at the GUV center, and the center positions were determined by fitting Gaussian functions to the profile. The two maxima define the positions of the GUV contact area and the upper membrane of the GUV. The contact radius R_i was calculated from the circular contact area that was measured by threshold analysis. To determine the radius R_{ad} of the spherical cap after adhesion, the circular equatorial plane of each adhered GUV was determined.

Reflectometric Interference Spectroscopy—Reflectometric interference spectroscopy measurements were performed using a custom-built setup equipped with a NanoCalc-2000 spectrometer (OceanOptics Germany GmbH, Ostfildern, Germany) (60). SiO_2 wafers with an oxide layer of 5 μm were incubated in a solution of NH_3 and H_2O_2 ($H_2O/NH_3/H_2O_2$, 5:1:1) for 20 min at 70 °C. The time course of bilayer formation after the addition of small unilamellar vesicles obtained by sonication (61) was monitored until a stable optical thickness was reached. After rinsing with buffer, the resulting

membrane was treated with a bovine serum albumin solution (1 mg/ml) to prevent nonspecific protein adsorption. After again rinsing with buffer, ENTH was added, and spectra were recorded every 2 s and the optical thickness determined (60).

Appendix

The free energy F_v of a vesicle adhering to a surface in the strong adhesion limits is given by Equation 1. Minimizing the free energy F_v leads to the following equilibrium condition,

$$\gamma_{ad} = K_A(1 - \cos\theta)\left(\frac{3 - \cos\theta}{(2(1 + \cos\theta)^{\frac{1}{2}}(2 - \cos\theta))^{\frac{2}{3}}} - 1\right) \quad \text{(Eq. 5)}$$

with $\theta = \sin^{-1}(R_i/R_{ad})$ (31). Adhesion energies larger than 10^{-4} J/m^2 were calculated for vesicles adhering to an avidin-coated glass surface based on the vesicle geometry using Equation 5 and $K_A = 0.265$ N/m (30, 42). Adhesion energies of $1.25{\cdot}10^{-4}$ J/m^2, $3.32{\cdot}10^{-4}$ J/m^2, $4.78{\cdot}10^{-4}$ J/m^2, and $7.70{\cdot}10^{-4}$ J/m^2 at Mg^{2+} concentrations of 0.5, 1, 2, and 3 mM, respectively, were determined in accordance with the assumption of the limit of strong adhesion.

An increase in R_i was measured as a result of ENTH binding, and we assume that helix-0 insertion into the bilayer enlarges the vesicle's surface area by δA_{ENTH}. Equation 1 can then be rewritten to,

$$F_{v,ENTH} = \frac{1}{2}K_A - \frac{((A_{ad} + \delta A_{ENTH,ad}) - (A_v + \delta A_{ENTH,v}))^2}{(A_v + \delta A_{ENTH,v})} - A_i\gamma_{ad} \quad \text{(Eq. 6)}$$

$\delta A_{ENTH,ad}$ denotes the area change of an adhered vesicle due to ENTH helix-0 insertion, whereas $\delta A_{ENTH,v}$ is the corresponding change in area of a free vesicle. Rearranging Equation 6 assuming $\delta A_{ENTH,ad} \cong \delta A_{ENTH,v} \cong \delta A_{ENTH}$ yields,

$$F_{v,ENTH} = \frac{1}{2}K_{A,ENTH}\frac{(A_{ad} - A_v)^2}{A_v} - A_i\gamma_{ad} \quad \text{(Eq. 7)}$$

with an apparent area compressibility modulus $K_{A,ENTH}$ after ENTH binding of,

$$K_{A,ENTH} = K_A\frac{A_v}{A_v + \delta A_{ENTH}} \quad \text{(Eq. 8)}$$

Assuming a constant adhesion energy γ_{ad} before and after ENTH addition, $K_{A,ENTH}$ can be obtained from,

$$K_{A,ENTH} = \frac{\gamma_{ad}}{(1 - \cos\theta_{ENTH})\left(\frac{3 - \cos\theta_{ENTH}}{2((1 + \cos\theta_{ENTH})^{\frac{1}{2}}(2 - \cos\theta_{ENTH}))^{\frac{2}{3}}} - 1\right)} \quad \text{(Eq. 9)}$$

where θ_{ENTH} is the equilibrium contact angle after ENTH addition. A mean apparent area compressibility modulus of $K_{A,ENTH} = 0.145 \pm 0.009$ N/m after ENTH addition was calculated for 3 initial lateral membrane tensions. The necessary change in vesicle area caused by binding of ENTH (δA_{ENTH}) required for a reduction of $K_A = 0.265$ N/m to the apparent area compressibility modulus $K_{A,ENTH} = 0.145$ N/m was then calculated using Equation 9. An area increase caused by helix-0 insertion of ENTH of 83% would be required to explain the observed reduction in the apparent area compressibility modulus while keeping K_A constant. This is unrealistic, as the relative area increase caused by the insertion of the ENTH helix was approximated to be 1–3% based on the protein's crystal structure. Therefore, the insertion of the ENTH helix is believed to cause the observed change of the area compressibility modulus neglecting the small change in area as a result of helix-0 insertion. The decrease in K_A translates into a reduction of the bending rigidity, i.e. a softening of the membrane as observed after insertion of helical peptides into lipid bilayers (53–55).

Author Contributions—M. G. performed the GUV experiments and analyzed the data. C. F. and N. T. performed the reflectometric interference spectroscopy experiments. B. K. and M. M. expressed and purified the proteins. T.-T. K. established the GUV adhesion mediated by Mg^{2+}. A. J. devised the theoretical model. C. S. and M. M. designed the experiments and wrote the manuscript. All authors reviewed the results and approved the final version of the manuscript.

Acknowledgment—M. G. thanks the Göttingen Graduate School for Neurosciences, Biophysics, and Molecular Biosciences for financial support.

References

1. Le Roy, C., and Wrana, J. L. (2005) Clathrin- and non-clathrin-mediated endocytic regulation of cell signalling. *Nat. Rev. Mol. Cell Biol.* **6,** 112–126
2. Doherty, G. J., and McMahon, H. T. (2009) Mechanisms of endocytosis. *Annu. Rev. Biochem.* **78,** 857–902
3. Weinberg, J., and Drubin, D. G. (2012) Clathrin-mediated endocytosis in budding yeast. *Trends Cell Biol.* **22,** 1–13
4. Boettner, D. R., Chi, R. J., and Lemmon, S. K. (2012) Lessons from yeast for clathrin-mediated endocytosis. *Nat. Cell Biol.* **14,** 2–10
5. Morris, C. E., and Homann, U. (2001) Cell surface area regulation and membrane tension. *J. Membr. Biol.* **179,** 79–102
6. Schweitzer, Y., Lieber, A. D., Keren, K., and Kozlov, M. M. (2014) Theoretical analysis of membrane tension in moving cells. *Biophys. J.* **106,** 84–92
7. Pietuch, A., Brückner, B. B. R., Fine, T., Mey, I., and Janshoff, A. (2013) Elastic properties of cells in the context of confluent cell monolayers: impact of tension and surface area regulation. *Soft Matter* **9,** 11490–11502
8. Lieber, A. D., Yehudai-Resheff, S., Barnhart, E. L., Theriot, J. A., and Keren, K. (2013) Membrane tension in rapidly moving cells is determined by cytoskeletal forces. *Curr. Biol.* **23,** 1409–1417
9. Raucher, D., and Sheetz, M. P. (1999) Membrane expansion increases endocytosis rate during mitosis. *J. Cell Biol.* **144,** 497–506
10. Dai, J., Ting-Beall, H. P., and Sheetz, M. P. (1997) The secretion-coupled endocytosis correlates with membrane tension changes in RBL 2H3 cells. *J. Gen. Physiol.* **110,** 1–10
11. Girao, H., Geli, M. I., and Idrissi, F. Z. (2008) Actin in the endocytic pathway: from yeast to mammals. *FEBS Lett.* **582,** 2112–2119
12. Boulant, S., Kural, C., Zeeh, J.-C., Ubelmann, F., and Kirchhausen, T. (2011) Actin dynamics counteract membrane tension during clathrin-mediated endocytosis. *Nat. Cell Biol.* **13,** 1124–1131
13. Kishimoto, T., Sun, Y., Buser, C., Liu, J., Michelot, A., and Drubin, D. G. (2011) Determinants of endocytic membrane geometry, stability, and scission. *Proc. Natl. Acad. Sci. U.S.A.* **108,** E979–E988
14. Mooren, O. L., Galletta, B. J., and Cooper, J. A. (2012) Roles for actin assembly in endocytosis. *Annu. Rev. Biochem.* **81,** 661–686
15. Doherty, G. J., and McMahon, H. T. (2008) Mediation, modulation, and

consequences of membrane-cytoskeleton interactions. *Annu. Rev. Biophys.* **37,** 65–95
16. Rauch, C., and Farge, E. (2000) Endocytosis switch controlled by transmembrane osmotic pressure and phospholipid number asymmetry. *Biophys. J.* **78,** 3036–3047
17. Diz-Muñoz, A., Fletcher, D. A., and Weiner, O. D. (2013) Use the force: membrane tension as an organizer of cell shape and motility. *Trends Cell Biol.* **23,** 47–53
18. Legendre-Guillemin, V., Wasiak, S., Hussain, N. K., Angers, A., and McPherson, P. S. (2004) ENTH/ANTH proteins and clathrin-mediated membrane budding. *J. Cell Sci.* **117,** 9–18
19. Lundmark, R., and Carlsson, S. R. (2010) Driving membrane curvature in clathrin-dependent and clathrin-independent endocytosis. *Semin. Cell Dev. Biol.* **21,** 363–370
20. Rozovsky, S., Forstner, M. B., Sondermann, H., and Groves, J. T. (2012) Single molecule kinetics of ENTH binding to lipid membranes. *J. Phys. Chem. B* **116,** 5122–5131
21. Stahelin, R. V., Long, F., Peter, B. J., Murray, D., De Camilli, P., McMahon, H. T., and Cho, W. (2003) Contrasting membrane interaction mechanisms of AP180 N-terminal homology (ANTH) and epsin N-terminal homology (ENTH) domains. *J. Biol. Chem.* **278,** 28993–28999
22. Yoon, Y., Tong, J., Lee, P. J., Albanese, A., Bhardwaj, N., Källberg, M., Digman, M. A., Lu, H., Gratton, E., Shin, Y. K., and Cho, W. (2010) Molecular basis of the potent membrane-remodeling activity of the epsin 1 N-terminal homology domain. *J. Biol. Chem.* **285,** 531–540
23. Boucrot, E., Pick, A., Çamdere, G., Liska, N., Evergren, E., McMahon, H. T., and Kozlov, M. M. (2012) Membrane fission is promoted by insertion of amphipathic helices and is restricted by crescent BAR domains. *Cell* **149,** 124–136
24. Ungewickell, E. J., and Hinrichsen, L. (2007) Endocytosis: clathrin-mediated membrane budding. *Curr. Opin. Cell Biol.* **19,** 417–425
25. Ford, M. G., Mills, I. G., Peter, B. J., Vallis, Y., Praefcke, G. J., Evans, P. R., and McMahon, H. T. (2002) Curvature of clathrin-coated pits driven by epsin. *Nature* **419,** 361–366
26. Kweon, D.-H., Shin, Y.-K., Shin, J. Y., Lee, J.-H., Lee, J.-B., Seo, J.-H., and Kim, Y. S. (2006) Membrane topology of helix 0 of the epsin N-terminal homology domain. *Mol. Cells* **21,** 428–435
27. Gleisner, M., Mey, I., Barbot, M., Dreker, C., Meinecke, M., and Steinem, C. (2014) Driving a planar model system into the 3(rd) dimension: generation and control of curved pore-spanning membrane arrays. *Soft Matter* **10,** 6228–6236
28. Albersdörfer, A., Feder, T., and Sackmann, E. (1997) Adhesion-induced domain formation by interplay of long-range repulsion and short-range attraction force: a model membrane study. *Biophys. J.* **73,** 245–257
29. Lipowsky, R., and Seifert, U. (1991) Adhesion of vesicles and membranes. *Mol. Cryst. Liq. Cryst.* **202,** 17–25
30. Gruhn, T., Franke, T., Dimova, R., and Lipowsky, R. (2007) Novel method for measuring the adhesion energy of vesicles. *Langmuir* **23,** 5423–5429
31. Ramachandran, A., Anderson, T. H., Leal, L. G., and Israelachvili, J. N. (2011) Adhesive interactions between vesicles in the strong adhesion limit. *Langmuir* **27,** 59–73
32. Rädler, J., and Sackmann, E. (1993) Imaging optical thicknesses and separation distances of phospholipid vesicles at solid surfaces. *J. Phys. II* **3,** 727–748
33. Shindell, O., Mica, N., Ritzer, M., and Gordon, V. (2015) Specific adhesion of membranes simultaneously supports dual heterogeneities in lipids and proteins. *Phys. Chem. Chem. Phys.* **17,** 15598–15607
34. Seantier, B., and Kasemo, B. (2009) Influence of mono- and divalent ions on the formation of supported phospholipid bilayers via vesicle adsorption. *Langmuir* **25,** 5767–5772
35. Puu, G., and Gustafson, I. (1997) Planar lipid bilayers on solid supports from liposomes-factors of importance for kinetics and stability. *Biochim. Biophys. Acta.* **1327,** 149–161
36. Ross, M., Steinem, C., Galla, H,-J. J., and Janshoff, A. (2001) Visualization of chemical and physical properties of calcium-induced domains in DPPC/DPPS Langmuir-Blodgett layers. *Langmuir* **17,** 2437–2445
37. Ekeroth, J., Konradsson, P., and Höök, F. (2002) Bivalent-ion-mediated vesicle adsorption and controlled supported phospholipid bilayer formation on molecular phosphate and sulfate layers on gold. *Langmuir* **18,** 7923–7929
38. Holmberg, A., Blomstergren, A., Nord, O., Lukacs, M., Lundeberg, J., and Uhlén, M. (2005) The biotin-streptavidin interaction can be reversibly broken using water at elevated temperatures. *Electrophoresis* **26,** 501–510
39. Bernard A-L, Guedeau-Boudeville M-A, Jullien, L., and Di Meglio, J. M. (2000) Strong adhesion of giant vesicles on surfaces: dynamics and permeability. *Langmuir* **16,** 6809–6820
40. Helfrich, W. (1973) Elastic properties of lipid bilayers - theory and possible experiments. *Z. Naturforsch. C* **28,** 693–703
41. Evans, E., and Rawicz, W. (1990) Entropy-driven tension and bending elasticity in condensed-fluid membranes. *Phys. Rev. Lett.* **64,** 2094–2097
42. Rawicz, W., Olbrich, K. C., McIntosh, T., Needham, D., and Evans, E. (2000) Effect of chain length and unsaturation on elasticity of lipid bilayers. *Biophys. J.* **79,** 328–339
43. Schäfer, E., Vache, M., Kliesch T.-T., and Janshoff, A. (2015) Mechanical response of adherent giant liposomes to indentation with a conical AFM-tip. *Soft Matter* **11,** 4487–4495
44. Rädler, J. O., Feder, T. J., Strey, H. H., and Sackmann, E. (1995) Fluctuation analysis of tension-controlled undulation forces between giant vesicles and solid substrates. *Phys. Rev. E* **51,** 4526–4536
45. Horvath, C. A., Vanden Broeck, D., Boulet, G. A., Bogers, J., and De Wolf, M. J. (2007) Epsin: inducing membrane curvature. *Int. J. Biochem. Cell Biol.* **39,** 1765–1770
46. Wood, L. A., and Royle, S. J. (2015) Zero tolerance: amphipathic helices in endocytosis. *Dev. Cell* **33,** 119–120
47. Kirchhausen, T. (2012) Bending membranes. *Nat. Cell Biol.* **14,** 906–908
48. Lai, C. L., Jao, C. C., Lyman, E., Gallop, J. L., Peter, B. J., McMahon, H. T., Langen, R., and Voth, G. A. (2012) Membrane binding and self-association of the epsin N-terminal homology domain. *J. Mol. Biol.* **423,** 800–817
49. Shi, Z., and Baumgart, T. (2015) Membrane tension and peripheral protein density mediate membrane shape transitions. *Nat. Commun.* **6,** 5974
50. Stachowiak, J. C., Schmid, E. M., Ryan, C. J., Ann, H. S., Sasaki, D. Y., Sherman, M. B., Geissler, P. L., Fletcher, D. A., and Hayden, C. C. (2012) Membrane bending by protein-protein crowding. *Nat. Cell Biol.* **14,** 944–949
51. Kozlov, M. M., Campelo, F., Liska, N., Chernomordik, L. V., Marrink, S. J., and McMahon, H. T. (2014) Mechanisms shaping cell membranes. *Curr. Opin. Cell Biol.* **29,** 53–60
52. Nagle, J. F., and Tristram-Nagle, S. (2000) Structure of lipid bilayers. *Biochim. Biophys. Acta.* **1469,** 159–195
53. Settles, E. I., Loftus, A. F., McKeown, A. N., and Parthasarathy, R. (2010) The vesicle trafficking protein Sar1 lowers lipid membrane rigidity. *Biophys. J.* **99,** 1539–1545
54. Bouvrais, H., Méléard, P., Pott, T., Jensen, K. J., Brask, J., and Ipsen, J. H. (2008) Softening of POPC membranes by magainin. *Biophys. Chem.* **137,** 7–12
55. Tristram-Nagle, S., and Nagle, J. F. (2007) HIV-1 fusion peptide decreases bending energy and promotes curved fusion intermediates. *Biophys. J.* **93,** 2048–2055
56. Campelo, F., McMahon, H. T., and Kozlov, M. M. (2008) The hydrophobic insertion mechanism of membrane curvature generation by proteins. *Biophys. J.* **95,** 2325–2339
57. Safari, F., and Suetsugu, S. (2012) The BAR domain superfamily proteins from subcellular structures to human diseases. *Membranes (Basel)* **2,** 91–117
58. Tourdot, R. W., Ramakrishnan, N., Baumgart, T., and Radhakrishnan, R. (2015) Application of a free energy landscape approach to study tension dependent bilayer tubulation mediated by curvature. *Phys. Rev. E* **92,** 042715
59. Simunovic, M., and Voth, G. A. (2015) Membrane tension controls the assembly of curvature-generating proteins. *Nat. Commun.* **6,** 7219
60. Stephan, M., Kramer, C., Steinem, C., and Janshoff, A. (2014) Binding assay for low molecular weight analytes based on reflectometry of absorbing molecules in porous substrates. *Analyst.* **139,** 1987–1992
61. Johnson, S. M., Bangham, A. D., Hill, M. W., and Korn, E. D. (1971) Single bilayer liposomes. *Biochim. Biophys. Acta* **233,** 820–826